

A dual-Helmholtz-coil magnetic field system for polarized ^{3}He

Jian Tang(唐健), Zecong Qin(秦泽聪), Yunfei Li(李云飞), Long Tian(田龙), Bin Wang(王斌), Qingbo Zheng(郑清波), Yujie Zheng(郑玉杰), Junsong Xie(谢俊松), Han Gao(高寒), Yuan Yao(姚远), Jun Li(李君), Tianhao Wang(王天昊), Junpei Zhang(张俊佩), and Xin Tong(童欣)

Citation: Chin. Phys. B, 2026, 35 (**7**): 070704. DOI: 10.1088/1674-1056/ae4580
http://cpb.iphy.ac.cn; http://iopscience.iop.org/cpb

What follows is a list of articles you may be interested in

High-sensitivity spectroscopic measurements under pulsed high magnetic field

Zheng Wang(王政), Yichun Pan(潘议淳), Guangran Yang(杨光冉), Wei Xie(谢微), and Weihang Zhou(周伟航)
Chin. Phys. B, 2025, 34 (**7**): 070701. DOI: 10.1088/1674-1056/adce95

Realization of an optimized cylindrical uniform magnetic field coil via flexible printed circuit technology

A-Hui Zhao(赵阿慧), Yong-Le Zhang(张永乐), Yue-Yue Liang(梁跃跃), Yi Zhang(张艺), Jun-Jun Zha(查君君), Dao-Rong Rui(芮道荣), Xiao-Qiang Zhang(张肖强), and Kang Yang(杨康)
Chin. Phys. B, 2024, 33 (**12**): 120702. DOI: 10.1088/1674-1056/ad84c1

Response optimization of a three-axis sensitive SERF magnetometer for closed-loop operation

Yuanrui Zhou(周原锐), Yongze Sun(孙永泽), Xixi Wang(汪茜茜), Jianan Qin(秦佳男), Xue Zhang(张雪), and Yanzhang Wang(王言章)
Chin. Phys. B, 2024, 33 (**2**): 020701. DOI: 10.1088/1674-1056/ad0b00

Magnetic shielding property for cylinder with circular, square, and equilateral triangle holes

Si-Yuan Hao(郝思源), Xiao-Ping Lou(娄小平), Jing Zhu(祝静), Guang-Wei Chen(陈广伟), and Hui-Yu Li(李慧宇)
Chin. Phys. B, 2021, 30 (**6**): 060702. DOI: 10.1088/1674-1056/abeeee

Magnetic field analysis in a diamond anvil cell for Meissner effect measurement by using the diamond NV^- center

Lin Zhao(赵琳), Donghui Yue(岳冬辉), Cailong Liu(刘才龙), Min Wang(王敏), Yonghao Han(韩永昊), Chunxiao Gao(高春晓)
Chin. Phys. B, 2019, 28 (**3**): 030702. DOI: 10.1088/1674-1056/28/3/030702

INSTRUMENTATION AND MEASUREMENT

A dual-Helmholtz-coil magnetic field system for polarized ^{3}He

Jian Tang(唐健)[1,2,3,4], Zecong Qin(秦泽聪)[1,2,4], Yunfei Li(李云飞)[1,2], Long Tian(田龙)[1,2,4], Bin Wang(王斌)[1,2,4,5], Qingbo Zheng(郑清波)[1,2,3,4], Yujie Zheng(郑玉杰)[1,2,4], Junsong Xie(谢俊松)[1,2,4], Han Gao(高寒)[1,2,6], Yuan Yao(姚远)[1,2,7], Jun Li(李君)[1,2,4], Tianhao Wang(王天昊)[1,2,3,4,†], Junpei Zhang(张俊佩)[1,2,3,4,‡], and Xin Tong(童欣)[1,2,3,4,§]

[1] *Institute of High Energy Physics, Chinese Academy of Sciences (CAS), Beijing* 100049, *China*
[2] *Spallation Neutron Source Science Center, Dongguan* 523803, *China*
[3] *School of Nuclear Science and Technology, University of Chinese Academy of Sciences, Beijing* 100049, *China*
[4] *Guangdong Provincial Key Laboratory of Extreme Conditions, Dongguan* 523803, *China*
[5] *Center for Neutron Science and Technology, Guangdong Provincial Key Laboratory of Magnetoelectric Physics and Devices, School of Physics, Sun Yat-Sen University, Guangzhou* 510275, *China*
[6] *Center for Neutron Scattering and Advanced Light Sources, Dongguan University of Technology, Dongguan* 523808, *China*
[7] *Sino-French Institute of Nuclear Engineering and Technology, Sun Yat-Sen University, Zhuhai* 519082, *China*

(Received 20 November 2025; revised manuscript received 23 January 2026; accepted manuscript online 13 February 2026)

This study focuses on developing a dual-Helmholtz-coil magnetic field system for polarized ^{3}He to generate a uniform magnetic field. A theoretical analysis of the mechanism by which dual Helmholtz coils produce a uniform magnetic field was first conducted. Based on these findings, the magnetic device was designed with the finite element analysis software COMSOL, employing an optimization algorithm to efficiently set current densities and minimize the transverse gradient in the central region. The simulated transverse gradient achieved was 9.54×10^{-5} cm^{-1} in the 20 cm×20 cm×8 cm central region, and the experimental measurement yielded a value of 6.31×10^{-4} cm^{-1}. Additionally, lifetime testing of two polarized ^{3}He cells revealed lifetimes of 151.0±1.8 h and 206.2±4.4 h, demonstrating the excellent magnetic field uniformity of the device. The current work integrates theoretical, simulated, and experimental results. It advances polarized ^{3}He magnetic technology, offers an upgrade solution for *off situ* polarized ^{3}He pumping stations to extend the volume of the uniform magnetic field without enlarging the coil size, and provides a method for using polarized ^{3}He on neutron beamlines requiring large acceptance angles.

Keywords: polarized ^{3}He, dual Helmholtz coils, magnetic field uniformity, finite element analysis, lifetime testing

PACS: 07.55.–w, 67.30.ep, 96.15.Gh

DOI: 10.1088/1674-1056/ae4580 **CSTR:** 32038.14.CPB.ae4580

1. Introduction

Polarized ^{3}He has a wide range of applications in particle physics and nuclear physics,[1,2] condensed matter physics,[3,4] nuclear magnetic resonance imaging,[5] magnetometry,[6,7] and polarized nuclear fusion fields.[8] Moreover, polarized ^{3}He can be used as a neutron spin filter (NSF) in polarized neutron experiments.[9–11] Currently, two commonly used methods for polarizing ^{3}He are spin-exchange optical pumping (SEOP)[12–15] and metastability-exchange optical pumping.[16] In these methods, the magnetic system primarily defines the polarization direction of ^{3}He and maintains its polarized state. Helmholtz coil magnetic field systems are employed to generate highly uniform magnetic fields, mainly in *off situ* polarized ^{3}He pumping systems[15] and wide-angle polarized ^{3}He devices.[17,18] Institutions such as ORNL,[19] NIST[20] and CSNS[21] have adopted single-pair Helmholtz coil designs for their *off situ* polarized ^{3}He pumping systems. Facilities including ISIS,[17] JCNS[18] and ILL[22,23] utilize a multi-pair Helmholtz coil configuration in the design of wide-angle polarized ^{3}He devices. Wide-angle polarized ^{3}He devices are essential for separating coherent, nuclear spin incoherent and magnetic scattering,[24] as well as for measuring magnetic excitations[25] and related phenomena. Typical neutron scattering experiments require a 10 cm diameter homogeneous field region. However, wide-angle cells often have an external diameter exceeding 20 cm,[26] a scale at which single-pair coils cannot meet the field-uniformity requirements. Therefore, advancing domestic wide-angle polarized ^{3}He NSF technology necessitates a magnetic field device capable of providing a large-volume uniform field, both for *off situ* pumping systems and for future wide-

†Corresponding author. E-mail: wangtianhao@ihep.ac.cn
‡Corresponding author. E-mail: zhangjunpei@ihep.ac.cn
§Corresponding author. E-mail: tongxin@ihep.ac.cn

© 2026 Chinese Physical Society and IOP Publishing Ltd. All rights, including for text and data mining, AI training, and similar technologies, are reserved.

angle polarized ^{3}He devices.

For a typical polarized ^{3}He pumping station, when the pumping stops, the ^{3}He polarization $P^0_{^3\mathrm{He}}(t=0)$ is gradually relaxed over time t in an exponential decaying form as described by

$$P_{^3\mathrm{He}}(t) = P^0_{^3\mathrm{He}} \exp\left(-\frac{t}{T_1}\right). \tag{1}$$

The relaxation time T_1 (also termed the lifetime) of polarized ^{3}He is influenced by three main factors:[27,28] wall collisions, magnetic dipole–dipole interactions, and magnetic field inhomogeneity, as shown below:

$$\frac{1}{T_1} = \Gamma_{\mathrm{r}} = \Gamma_{\mathrm{wall}} + \Gamma_{\mathrm{dipole\text{-}dipole}} + \Gamma_{\mathrm{gradient}} \tag{2}$$

$$\Gamma_{\mathrm{gradient}} = \frac{7000}{p}\frac{|\nabla B_x|^2 + |\nabla B_y|^2}{B_0^2}. \tag{3}$$

Here, p is the polarized ^{3}He gas pressure in bars. Once the polarized ^{3}He cell has been sealed, the first two factors remain fixed. Therefore, magnetic field uniformity becomes crucial for extending the relaxation time. Consequently, reducing the standardized transverse gradient $\sqrt{(|\nabla B_x|^2 + |\nabla B_y|^2)/B_0^2}$ is key to extending the relaxation time of polarized ^{3}He, and it should usually be reduced to the order of 10^{-4} cm^{-1}.

A common choice for generating a magnetic field in an *off situ* pumping station is to use a pair of Helmholtz coils.[19–21] However, to provide a standardized gradient on the order of 10^{-4} cm^{-1}, the size of the Helmholtz coils is usually so large that it increases the footprint of the *off situ* pumping station. To address this, this study investigates a nested dual-Helmholtz-coil configuration. Theoretical derivations demonstrate that the uniformity of dual Helmholtz coils is superior to that of a single pair of Helmholtz coils. Meanwhile, the finite element analysis (FEA) simulation software COMSOL[29] and its optimization module were used to determine electric current parameters to minimize the gradient in the central region (length × width × height = 20 cm × 20 cm × 8 cm). The nested dual Helmholtz coils were designed according to these simulation results. During the commissioning, a three-dimensional stepper motor combined with a gaussmeter was employed to map the magnetic field in the central region.

The novelty of the presented approach lies in its compact, nested dual-coil geometry combined with automated current-density optimization. In contrast to conventional designs that employ spatially separated main and compensation coils, the proposed system integrates two concentric Helmholtz pairs with opposing currents. This configuration promotes more effective cancellation of higher-order field gradients within a limited footprint. In simulation, a transverse gradient of 9.54×10^{-5} cm^{-1} is achieved in the target volume, which represents an order of magnitude improvement over a single Helmholtz pair (2.05×10^{-3} cm^{-1}). When evaluated under a fixed gradient threshold, the designed system provides approximately 2.5 times larger usable uniform field volume than conventional multi-coil designs, offering a distinct advantage for applications that require extended uniform fields without increasing the overall system scale. The performance of the dual-Helmholtz-coil design has also been experimentally validated. The lifetimes of two polarized ^{3}He cells are simultaneously measured by the free induction decay (FID) method.[30,31] Compared with a single pair of Helmholtz coils with the same diameter, this dual-Helmholtz-coil design significantly enlarges the central uniform region, making it suitable for upgrading the magnetic system on *off situ* pumping stations using the SEOP method. Moreover, the magnetic field design serves as a wide-angle polarized ^{3}He device, featuring a large neutron scattering angle.

2. The uniformity theory of dual Helmholtz coils

Guo[32] derived the magnetic field at the spatial point $P(r,\theta,\phi)$ for a pair of coils arranged on a sphere of radius R with current I. Equation (4) presents the expression of the magnetic field in cylindrical coordinates at point $P(\rho,\theta,z)$, and Fig. 1 illustrates the coil layout within this coordinate system:

$$\begin{aligned} B_z &= \frac{\mu I}{R}\sum_{n=0}^{\infty} \sin\alpha P^1_{2n+1}(\cos\alpha) P_{2n}(\cos\theta)\left(\frac{\rho^2+z^2}{R^2}\right)^n, \\ B_\rho &= -\frac{\mu I}{R}\sum_{n=0}^{\infty}\frac{1}{2n+1}\sin\alpha P^1_{2n+1}(\cos\alpha) P^1_{2n}(\cos\theta) \\ &\quad \times \left(\frac{\rho^2+z^2}{R^2}\right)^n, \\ B_\theta &= 0. \end{aligned} \tag{4}$$

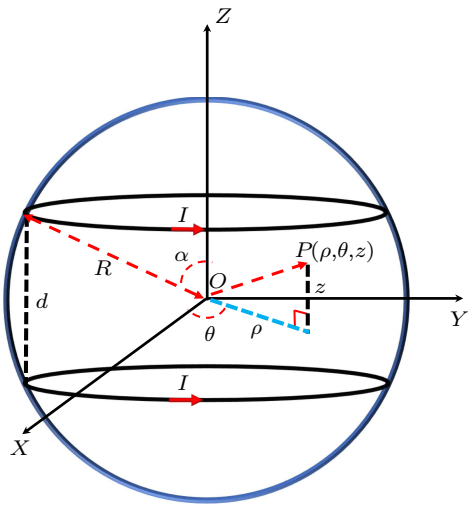


Fig. 1. Coil arrangement in the coordinate system.

To obtain the most uniform magnetic field in the central region, the coefficients of the expansion must be minimized.

The $n=0$ term provides a constant field, independent of ρ. The condition for nullifying the $n=1$ term is $\cos\alpha = 1/\sqrt{5}$, which leads to $B_\rho = 0$ and defines the classic Helmholtz coil configuration, where the coil radius $R\sin\alpha$ equals the separation distance d. The enhanced uniformity of the dual-Helmholtz-coil design is achieved through the systematic cancellation of higher-order magnetic field gradients. While a single Helmholtz pair minimizes the first-order (dipole) variation by satisfying $d=R$, it retains significant second-order (quadrupole) gradients. The limitation of a single Helmholtz pair design is overcome via a gradient superposition principle: two concentric coil pairs with opposing currents are configured so that their quadrupole contributions destructively interfere. To cancel the $n=2$ (quadrupole) term, a dual-coil system is employed. The total magnetic field is the superposition of the fields from two Helmholtz pairs with radii $R_1\sin\alpha$ and $R_2\sin\alpha$, carrying currents I_1 and I_2, respectively. The explicit forms of $B_{z1}, B_{z2}, B_{\rho1}, B_{\rho2}$ follow

$$
\begin{aligned}
B_z &= B_{z1} + B_{z2} \\
&= \frac{\mu I_1}{R_1}\sum_{n=0}^{\infty}\sin\alpha\, P_{2n+1}^1(\cos\alpha)P_{2n}(\cos\theta)\left(\frac{\rho^2+z^2}{R_1^2}\right)^n \\
&\quad + \frac{\mu I_2}{R_2}\sum_{n=0}^{\infty}\sin\alpha\, P_{2n+1}^1(\cos\alpha)P_{2n}(\cos\theta)\left(\frac{\rho^2+z^2}{R_2^2}\right)^n, \\
B_\rho &= B_{\rho1} + B_{\rho2} \\
&= -\frac{\mu I_1}{R_1}\sum_{n=0}^{\infty}\frac{1}{2n+1}\sin\alpha\, P_{2n+1}^1(\cos\alpha)P_{2n}^1(\cos\theta) \\
&\quad \times\left(\frac{\rho^2+z^2}{R_1^2}\right)^n \\
&\quad - \frac{\mu I_2}{R_2}\sum_{n=0}^{\infty}\frac{1}{2n+1}\sin\alpha\, P_{2n+1}^1(\cos\alpha)P_{2n}^1(\cos\theta) \\
&\quad \times\left(\frac{\rho^2+z^2}{R_2^2}\right)^n, \\
B_\theta &= B_{\theta1} + B_{\theta2} = 0,
\end{aligned}
\tag{5}
$$

with the corresponding radii and currents. To derive the cancellation condition for the $n=2$ term, the expansions of $B_{\rho1}$ and $B_{\rho2}$ are written explicitly. For the dual-coil system, the total B_ρ is the sum of two such series with parameters (I_1, R_1) and (I_2, R_2). The condition for canceling the $n=2$ term is that the sum of the $n=2$ contributions from both coils vanishes, i.e., $B_{\rho1} + B_{\rho2} = 0$. The $n=2$ term of each coil is proportional to I/R^5 and shares the same angular dependence. Explicitly, $B_{\rho1} \propto \frac{I_1}{R_1^5}\cdot\sin\alpha\, P_5^1(\cos\alpha)P_4^1(\cos\theta)$, $B_{\rho2} \propto \frac{I_2}{R_2^5}\cdot\sin\alpha\, P_5^1(\cos\alpha)P_4^1(\cos\theta)$. Setting the sum to zero and canceling the common non-zero factors (the angular part and $\sin\alpha$) yields the condition: $\frac{I_1}{R_1^5} + \frac{I_2}{R_2^5} = 0$.

Thus, when the currents in the two coil pairs satisfy this relation, the quadrupole ($n=2$) gradient is eliminated at the center. This allows the dual-Helmholtz-coil design to enhance the magnetic field uniformity while maintaining the same outer diameter as a single pair.

3. The design and simulation of dual Helmholtz coils

Based on the theoretical framework established in Section 2, the design and simulation stage was initiated. The primary objective was to translate the theoretical dual-coil concept into a practical magnetic field device and to optimize its performance using FEA.

A finite-element model of the dual-Helmholtz-coil system was established in COMSOL Multiphysics® [29] to ensure reproducible simulations. The coil geometry (Fig. 2) was constructed according to the parameters in Table 1, incorporating the actual rectangular cross-section of the windings (2 mm × 4 mm). The magnetostatic *Magnetic Fields* (mf) interface was applied within a spherical air domain of radius 3.0 m, sufficiently large to avoid boundary effects. The external boundary condition was set to *Magnetic Insulation* to simulate free-space conditions.

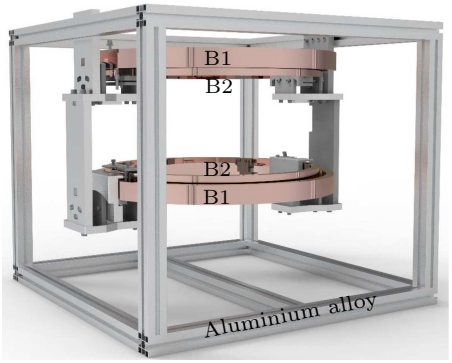


Fig. 2. Design of a dual Helmholtz coils magnetic system, supported by an aluminum alloy structure.

Table 1. Parameters of the dual Helmholtz coils: outer diameter (OD), inner diameter (ID), number of turns/layer (N_{turns}), number of layers (N_{layers}), and wire diameter (WD).

Coil	OD (cm)	ID (cm)	N_{turns}	N_{layers}	WD (mm^2)
B1	58.4	55.2	8	9	2×4
B2	51.2	48.0	8	8	2×4

A user-controlled free-tetrahedral mesh with an element size of 8 mm was applied in the coils and the central region of interest. Mesh independence was verified by recalculating the average transverse gradient in the central target region (20 cm × 20 cm × 8 cm) using a systematically refined mesh. The variation in the computed gradient was less than 0.3%, confirming that the chosen mesh yields grid-independent results.

First, initial parameters were set according to the theoretical analysis. The current density J_1 of coil B1 was fixed at 1.25 A/mm^2. The initial current density J_2 of coil B2 was determined from the theoretical condition $B_{\rho1} + B_{\rho2} = 0$, resulting in $J_2 = 0.71$ A/mm^2. Using this initial parameter set,

models of the B1 and B2 coils were built in COMSOL and simulated. This initial simulation gave a magnetic field of 9.6 G and an average volumetric gradient of 2.59×10^{-4} cm^{-1} in the central target region (20 cm × 20 cm × 8 cm). For reference, the theoretical (analytical) values for the dual-coil system at $J_2 = 0.71$ A/mm^2 are a central field of 9.6 G and a mean gradient of 1.34×10^{-4} cm^{-1} (from Eq. (5)) (Figs. 3(a) and 3(b)). The corresponding single-coil (B1 only) theoretical values at the same $J_1 = 1.25$ A/mm^2 are 22.1–22.8 G and 1.48×10^{-3} cm^{-1}, respectively (Figs. 3(c) and 3(d)). However, this initial simulated mean gradient, 2.59×10^{-4} cm^{-1}, was about 1.9 times larger than the purely theoretical prediction of 1.34×10^{-4} cm^{-1}. The discrepancy stems from the idealization of the coils as line currents in the theoretical model, whereas the actual coils possess a finite rectangular cross-section. This finite geometry alters the current distribution and the effective winding distance. Two primary effects arise: (1) the current is distributed over a finite volume, which modifies the magnetic field profile, particularly near the coil edges; and (2) the effective radial position of the windings relative to the central region is shifted. Collectively, these effects distort the field geometry, rendering the simple line-current model inadequate for precisely predicting the gradient within our target volume.

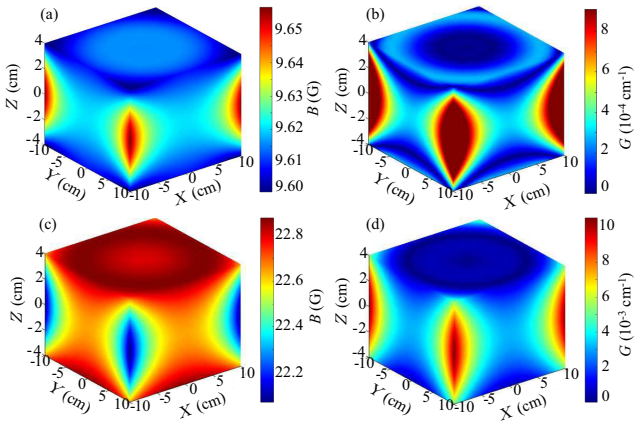


Fig. 3. Calculated magnetic field in the central region (20 cm×20 cm×8 cm). (a) Magnetic field strength of 9.6 G and (b) transverse volume gradient of 1.34×10^{-4} cm^{-1} for the dual Helmholtz coils, derived from analytical numerical solutions. For comparison, (c) and (d) show the corresponding analytical results for a single Helmholtz coil pair (B1 alone), exhibiting a magnetic field strength of 22.1–22.8 G and a transverse volume gradient of 1.48×10^{-3} cm^{-1}.

To compensate for the effects of the finite geometry, an automated optimization was performed. The optimization aimed to minimize the volume-averaged normalized transverse gradient in the central region, defined as the objective function:

$$f_{\text{obj}} = \frac{1}{V}\int_V \sqrt{\frac{|\nabla B_x|^2 + |\nabla B_y|^2}{B_0^2}}\,\mathrm{d}V, \tag{6}$$

where V is the volume of the central region. The optimization was performed using COMSOL's built-in COBYLA (Constrained Optimization BY Linear Approximation) algorithm. The current density for coil B1 was fixed at 1.25 A/mm^2; the current density J_2 of coil B2 (initial value 0.71 A/mm^2) served as the optimization variable, constrained within ±3 A/mm^2 of its initial value. The convergence criterion was set to a relative change in f_{obj} of less than 1×10^{-6}. The algorithm converged to an optimal current density $J_2 = 0.68$ A/mm^2, representing a 4.2% adjustment from the theoretical starting point. This adjustment effectively rebalances the magnetic contributions of the two coils, counteracting the distortion caused by their finite size. A final simulation with the optimized parameters ($J_1 = 1.25$ A/mm^2, $J_2 = 0.68$ A/mm^2) yielded significantly improved results: a central field of 10.1 G and a much-reduced mean gradient of 9.54×10^{-5} cm^{-1} (Figs. 4(a) and 4(b)). For comparison, a single pair of B1 Helmholtz coils operated at a current density of 1.25 A/mm^2 was also simulated (Figs. 4(c) and 4(d)). The single-coil system produced a field of 22.1–22.8 G and a mean transverse gradient of 2.05×10^{-3} cm^{-1} in the same central region. Clearly, the dual-Helmholtz-coil configuration provides a substantially more uniform magnetic environment than a single coil pair.

ISIS[17] and ILL[22] also employed two sets of coil designs to create magnetic field devices. For a typical Helmholtz coil, a uniform region is rendered at the center of its region, proportional to the size of the coil itself. Therefore, it is impossible to directly compare the magnetic field systems. A dimensionless figure of merit, denoted as A, is defined and employed here as the ratio of two volumes: the volume within which the magnetic field gradient at the device center is less than or equal to a fixed gradient threshold ($\sim 10^{-4}$ cm^{-1}) and the total volume occupied by the magnetic field device itself.

The ISIS magnetic system comprises a main coil pair (outer diameter 695 mm, 300 turns) and a counter-wound compensation pair (outer diameter 416 mm, 69 turns), with axial separations of 334 mm (compensation) and 410 mm (main). The cell-placement region is a cylinder with an internal diameter of 10 cm, an external diameter of 24 cm, and a height of 17 cm. A COMSOL model of this setup was constructed, and the average gradient within the cell position region was optimized, yielding a best value of 7.97×10^{-4} cm^{-1}, consistent with the reported performance of the ISIS device (8×10^{-4} cm^{-1}). Subsequently, the volume corresponding to a gradient $\leq 10\times10^{-4}$ cm^{-1} was simulated. Figure 5 shows the transverse gradient distribution in the $Z = 0$ plane, with the red contour marking the 10×10^{-4} cm^{-1} level. Panel (a) corresponds to the ISIS model, yielding $A_{\text{ISIS}} = 5.39\%$, while panel (b) shows our dual-Helmholtz-coil model, for which $A_{\text{dual}} = 13.26\%$. This result indicates that, for the same overall device volume, the uniform-field region of the dual-Helmholtz-coil design is about 2.5 times larger than that of the ISIS style system.

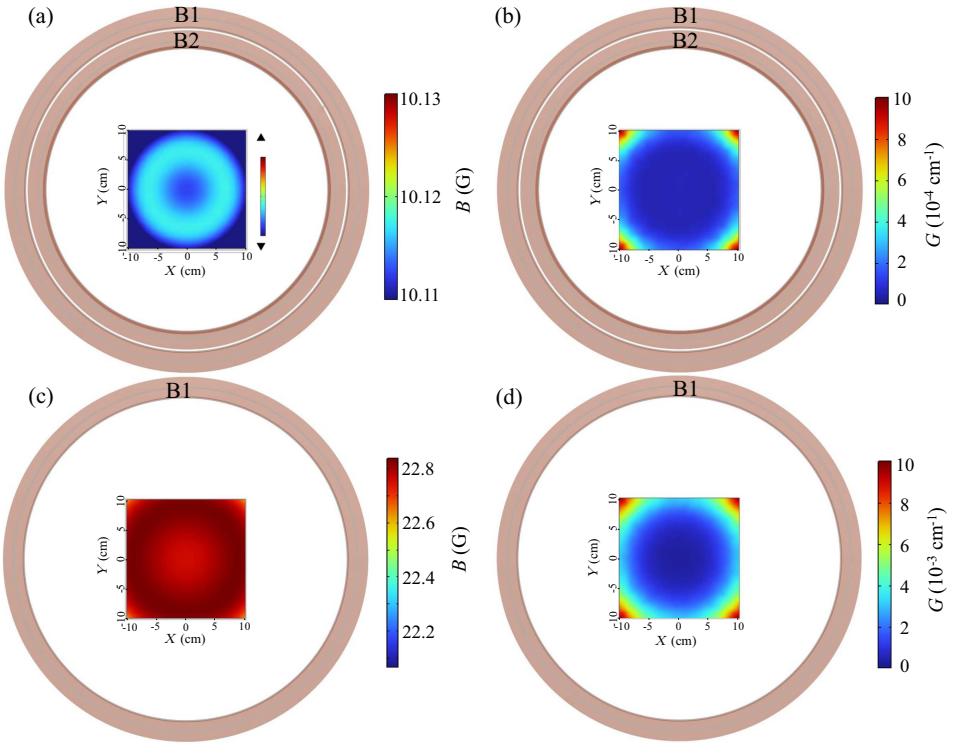


Fig. 4. Simulated magnetic field in the central region (20 cm×20 cm×8 cm) (top view). (a) Magnetic field strength of 10.1 G and (b) transverse volume gradient of 9.54×10^{-5} cm^{-1} for the optimized dual Helmholtz coils. For comparison, (c) and (d) present corresponding results for the single Helmholtz coil pair (B1 configuration), exhibiting a magnetic field strength of 22.1–22.8 G and transverse volume gradient of 2.05×10^{-3} cm^{-1}.

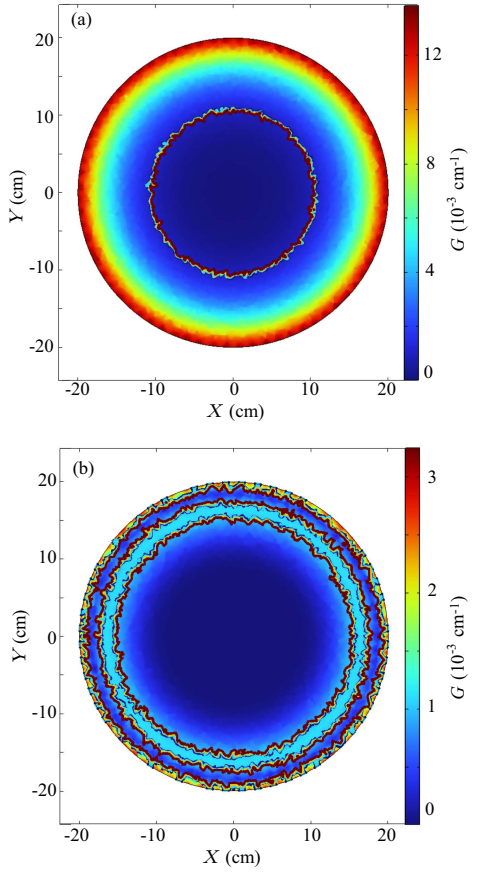


Fig. 5. (a) The transverse gradient distribution in the $Z = 0$ plane for the ISIS magnetic field model. (b) The transverse gradient distribution in the $Z = 0$ plane for the dual-Helmholtz-coil magnetic field model.

The comparison above relies on a fixed gradient threshold (10×10^{-4} cm^{-1}) to define the uniform field boundary. To verify that the concluded advantage is not an artifact of this particular choice, the sensitivity of the volume ratio $A_{\rm dual}/A_{\rm ISIS}$ to the threshold value was examined. The ratio remains between 2.3 and 4.0 across a wide range of thresholds from 1.0×10^{-3} cm^{-1} down to 1.0×10^{-4} cm^{-1}, with a value of 2.5 at the originally selected threshold. This confirms that the dual-Helmholtz-coil configuration consistently provides a substantially larger uniform field volume, and the conclusion is robust against variations in the defining gradient criterion.

4. Uniformity measurements of dual Helmholtz coils

Following the simulation-guided design and optimization described in Section 3, the dual-Helmholtz-coil system was fabricated and experimentally characterized. This section aims to validate the predicted field uniformity through direct magnetic field mapping and, more importantly, by measuring the relaxation lifetime of polarized ^{3}He cells — a direct indicator of field quality. The B1 and B2 coils were wound according to the parameters in Table 1 and fixed with epoxy resin approximately 1.8 mm thick. The corresponding mechanical supports and adjustment mechanisms for the B1 and B2 coils were designed based on Fig. 2(a). The mechanical design allows the central heights of the B1 and B2 coils to be adjusted within ±3 mm of the theoretical design value. It also enables each coil to rotate ±3° around the z-axis. After the magnetic field device was designed, fabricated, and assembled, the mechanical positioning structure was used to

fine-tune the coil positions based on the actual magnetic field measurements. In addition, the currents in the B2 coils were carefully adjusted based on the test results of polarized ^{3}He. A three-dimensional stepper motor combined with a gaussmeter was used to measure the magnetic field. Measurements were performed in the central core region (20 cm×20 cm×8 cm) of the device, with a resolution of 5 mm in each direction. The measured magnetic field in the central core region was 10.1–10.2 G, with a mean volumetric transverse gradient of 6.31×10^{-4} cm^{-1} (Fig. 6). The difference from the simulated gradient (9.54×10^{-5} cm^{-1}) primarily arises from practical experimental factors. These include coil-positioning uncertainties (contributing up to $\sim 10^{-4} - 10^{-3}$ cm^{-1}), DC current ripple, environmental stray fields, and instrumental limitations of the gaussmeter. Controlled perturbation simulations confirm that the combined effect of these quantifiable tolerances is on the order of 10^{-4} cm^{-1}, consistent with the observed discrepancy. Hence, the deviation is attributable to typical experimental variations and does not undermine the design or simulation validity.

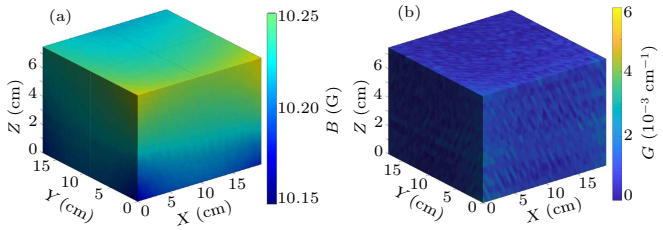


Fig. 6. (a) Measured magnetic field in the central region. (b) Measured magnetic field standardized transverse gradient in the central region.

After the actual magnetic field measurement, two polarized ^{3}He cells (Cell20221230 and Cell20230324), produced at the gas filling station at CSNS,[33] were used to test the magnetic field uniformity. Cell20221230 and Cell20230324 both have a diameter and length of 8.0 cm, with the cell wall thickness being approximately 0.4 cm. The pressures of Cell20221230 and Cell20230324 were determined by neutron transmission measurements according to[34–36]

$$T_0 = T_e \exp(-n\sigma l) = T_e \exp(-0.072 p\lambda \times l), \qquad (7)$$

where T_0 is the neutron transmission for the unpolarized ^{3}He, T_e is transmission through an empty glass, p is the ^{3}He pressure in bar, λ is the neutron wavelength in angstroms, and l is the path length inside the cell in centimeters. By plotting the neutron transmission as a function of wavelength (Fig. 7) and fitting using Eq. (7), the measurement results show that the pressures of Cell20221230 and Cell20230324 were 1.93 bar and 2.52 bar, respectively, at the room temperature of 25 °C. Subsequently, the lifetimes T_1 of the two cells were tested on the pumping station at CSNS,[21] which features a Helmholtz coil system with an outer diameter of 86 cm. Within the central region of the Helmholtz coils (10 cm×10 cm×10 cm), the mean transverse gradient simulated was 9.05×10^{-5} cm^{-1}, as shown in Fig. 8, and the measured mean volume transverse gradient was 5.8×10^{-4} cm^{-1}.[21] The lifetimes of Cell20221230 and Cell20230324, measured at the pumping station, were 165.1±1.4 h and 251.9±2.4 h, respectively. The measured lifetimes are shown in Fig. 9. Subsequently, the dual-Helmholtz-coil magnetic field device was used to test Cell 1 and Cell 2. The FID method[30,31] was used separately to pick up signals from Cell20221230 and Cell20230324. After acquiring the FID signal, the T_2 value of the FID signal quickly reflects the magnetic field uniformity at the FID coil position,[13] allowing an initial assessment of the magnetic field uniformity in the central region. Finally, the fitted lifetime T_1 was used to definitively determine the magnetic field uniformity.

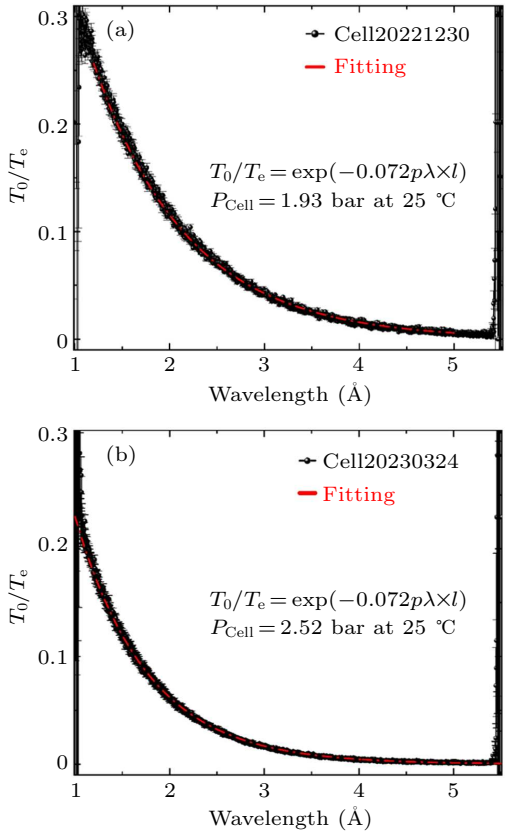


Fig. 7. Neutron calibration results of pressure in polarized ^{3}He cells: (a) Cell20221230 has a pressure of 1.93 bar and (b) Cell20230324 has a pressure of 2.52 bar.

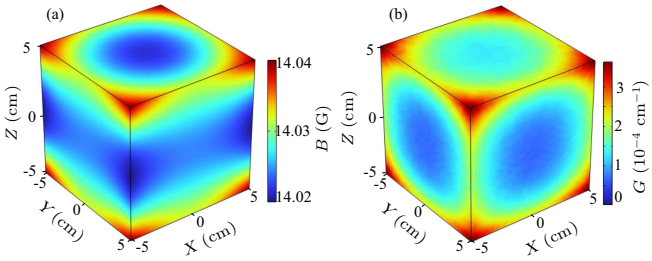


Fig. 8. (a) Simulated magnetic field in the central region (10 cm×10 cm×10 cm). (b) Simulated magnetic field standardized transverse gradient in the same region.

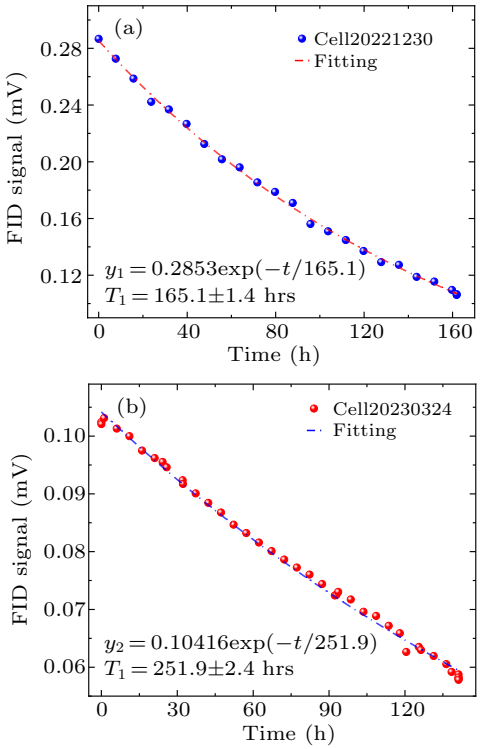


Fig. 9. (a) Fitting result of the lifetime of Cell20221230. (b) Fitting result of the lifetime of Cell20230324.

Subsequently, the two cells were placed in the dual Helmholtz coils for performance demonstration. Cell20221230, acting as the polarizer, was placed inside an aluminum alloy box, while Cell20230324, serving as the analyzer, was mounted on a bracket approximately 4 cm away from the box. The two cells together were centered in a region of 20 cm×20 cm×8 cm. The placement of Cell20221230 and Cell20230324 and the magnetic field device is shown in Fig. 10(a). The FID method[30,31] was used simultaneously to measure the signals from Cell20221230 and Cell20230324 and to fit T_1. Cell20221230 exhibited a lifetime of 151.0±1.8 h, while Cell20230324 demonstrated a lifetime of 206.2±4.4 h. The specific test results are shown in Fig. 10(b). The lifetimes measured in the dual-Helmholtz-coil system are close to those obtained on the filling station but present a decrease. This can be attributed to two aspects. In addition to the fact that the measured transverse magnetic field gradient is slightly higher than that of the filling station, the simultaneous FID measurements by employing two pick-up coils would have further altered the field uniformity and aggravated the polarization relaxation. On the other hand, the lifetimes measured in the dual-Helmholtz-coil system are sufficiently long, and the uniform field area is extended to one three times larger. Moreover, compared with conventional neutron beam transportation solenoid devices (neutron scattering angle $< 10°$),[21] this system achieves a much larger neutron acceptance angle of approximately 20°. These advantages make the current design suitable for future application on neutron beamlines.

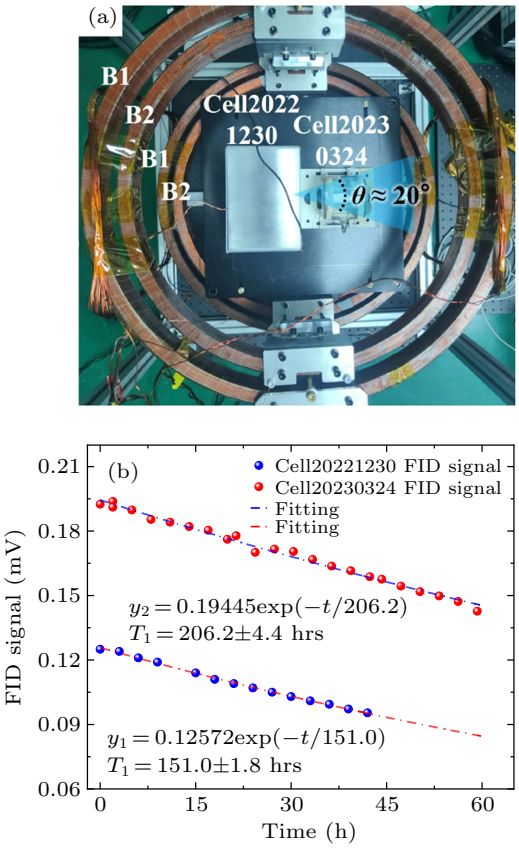


Fig. 10. (a) Test configuration of Cell20221230 and Cell20230324. (b) Fitting results of the lifetimes of Cell20221230 and Cell20230324.

5. Conclusion

Combining the theoretical, simulated, and experimental results presented in the preceding sections, we have successfully developed and validated a dual-Helmholtz-coil magnetic field system for polarized ^{3}He applications. The key findings and implications are summarized as follows. A dual Helmholtz magnetic field device for polarized ^{3}He was successfully proposed and developed, comprising two pairs of Helmholtz coils. Theoretical derivations show better uniformity in the dual coils than in a single pair with the same outer diameter. The dual-Helmholtz-coil system was designed using the FEA software COMSOL, where an optimization algorithm was employed to minimize the gradient in the central region. This resulted in a simulated magnetic field uniformity of 9.54×10^{-5} cm^{-1} within a 20 cm × 20 cm × 8 cm volume. The measured gradient of the final device was 6.31×10^{-4} cm^{-1}.

Finally, two polarized ^{3}He cells (Cell20221230 and Cell20230324) were placed in the device's central region for lifetime testing by the FID method. The lifetimes of the two cells were 151.0±1.8 h and 206.2±4.4 h, respectively. Combined with Cell20230324, the device enables a neutron scattering angle of approximately 20°. The magnetic field design offers a solution for *off situ* ^{3}He pumping stations to extend the volume of the uniform magnetic field without enlarging the size of the coils, and provides a method for using polarized

^{3}He on neutron beamlines requiring large acceptance angles.

Acknowledgments

This work was supported by the National Science Fund for Distinguished Young Scholars of China (Grant No. 12425512), the National Natural Science Foundation of China (Grant Nos. U2230207 and 11875265), the Guangdong Basic and Applied Basic Research Foundation (Grant No. 2019B1515120079), Guangdong Provincial Key Laboratory of Extreme Conditions (Grant No. 2023B1212010002), and Dongguan Polarized Neutron Key Laboratory.

References

[1] Jau Y Y, Hussey D S, Gentile T R and Chen W 2020 *Phys. Rev. Lett.* **125** 110801
[2] Zhang M, Yang Z, Zhang J, Huang C, Wang T, Chen Y, Fan R, Snow W M and Tong X 2025 *Nucl. Instrum. Methods Phys. Res. Sect. A* **1072** 170184
[3] Hang X, Matsuda M, Held J T, Mkhoyan K A and Wang J P 2020 *Phys. Rev. B* **102** 104402
[4] Krycka K, Borchers J, Ijiri Y, Booth R and Majetich S 2012 *Applied Crystallography* **45** 554
[5] Brunner E 1999 *Concepts in Magnetic Resonance: An Educational Journal* **11** 313
[6] Kraft A, Koch H C, Daum M, Heil W, Lauer T, Neumann D, Pazgalev A, Sobolev Y and Weis A 2014 *EPJ Techniques and Instrumentation* **1** 1
[7] Farooq M, Chupp T, Grange J, Tewsley-Booth A, Flay D, Kawall D, Sachdeva N and Winter P 2020 *Phys. Rev. Lett.* **124** 223001
[8] Baylor L, Deur A, Eidietis N, Heidbrink W W, Jackson G L, Liu J, Lowry M M, Miller G W, Pace D and Sandorfi A M 2023 *Nuclear Fusion* **63** 076009
[9] Coulter K, Chupp T, McDonald A, Bowman C, Bowman J, Szymanski J, Yuan V, Cates G, Benton D and Earle E 1990 *Nucl. Instrum. Methods Phys. Res. Sect. A* **288** 463
[10] Tasset F, Chupp T, Pique J, Steinhof A, Thompson A, Wasserman E and Ziade M 1992 *Physica B* **180** 896
[11] Gentile T R, Nacher P, Saam B and Walker T 2017 *Rev. Mod. Phys.* **89** 045004
[12] Zhang J, Huang C, Qin Z, Ye F, Amir S M, Salman A, Dong Y, Tian L, Buck Z N and Kreuzpaintner W 2022 *Science China Physics, Mechanics & Astronomy* **65** 241011
[13] Tang J, Wang B, Huang C, Gao H, Zheng Q, Liu R, Ye F, Qin Z, Wang T and Salman A 2025 *Chin. Phys. Lett.* **42** 022901
[14] Jiang C, McDonald L, Cao H, Balafas M, Crow L and Kroll E 2023 *J. Phys.: Conf. Ser.* **2481** 012010
[15] Yan S, Zhang M F, Guo W C, Wang W Z, Gong J, Liang T J, Liu B Q, Peng M, Peng S M and Sun G A 2019 *Science China Physics, Mechanics & Astronomy* **62** 102021
[16] Wang Y, Wu L, Zhang K, Peng M, Chen S and Yan H 2024 *Science China Physics, Mechanics & Astronomy* **67** 273011
[17] Cassella G, Stewart J, Paternò G, Sakai V G, Devonport M, Galsworthy P, Bewley R, Voneshen D, Raspino D and Nilsen G 2019 *J. Phys.: Conf. Ser.* **1316** 012007
[18] Voigt J, Soltner H, Babcock E, Aldus R J, Salhi Z, Gainov R R and Brückel T 2015 *EPJ Web of Conferences* **83** 03016
[19] Jiang C, Tong X, Brown D, Lee W, Ambaye H, Craig J, Crow L, Culbertson H, Goyette R and Graves-Brook M 2013 *Physics Procedia* **42** 191
[20] Chen W, Gentile T R, Erwin R, Watson S, Ye Q, Krycka K L and Maranville B B 2014 *J. Phys.: Conf. Ser.* **528** 012014
[21] Huang C, Zhang J, Ye F, Qin Z, Amir S M, Buck Z N, Salman A, Kreuzpaintner W, Qi X, Wang T, *et al.* 2021 *Chin. Phys. Lett.* **38** 092801
[22] Babcock E, Salhi Z, Pistel P, Simeoni G and Ioffe A 2014 *J. Phys.: Conf. Ser.* **528** 012018
[23] Jullien D, Petoukhov A, Enderle M, Thiery N, Mouveau P, Hansen U B, Chevalier P and Courtois P 2021 *Nucl. Instrum. Methods Phys. Res. Sect. A* **1010** 165558
[24] Steffens P, Sidis Y, Kulda J, Mao Z, Maeno Y, Mazin I and Braden M 2019 *Phys. Rev. Lett.* **122** 047004
[25] Do S H, Zhang H, Dahlbom D A, Williams T J, Garlea V O, Hong T, Jang T H, Cheong S W, Park J H and Barros K 2023 *npj Quantum Materials* **8** 5
[26] Chen W, Gentile T R, Ye Q, Kirchhoff A, Watson S, Rodriguez-Rivera J, Qiu Y and Broholm C 2016 *J. Phys.: Conf. Ser.* **746** 012016
[27] Petoukhov A, Guillard V, Andersen K, Bourgeat-Lami E, Chung R, Humblot H, Jullien D, Lelievre-Berna E, Soldner T, Tasset F, et al. 2006 *Nucl. Instrum. Methods Phys. Res. Sect. A* **560** 480
[28] Babcock E, Salhi Z, Barnsley L, Voigt J, Mattauch S and Ioffe A 2019 *J. Phys.: Conf. Ser.* **1316** 012019
[29] COMSOL AB 2023 Comsol multiphysics® 2023 v6.0 https://www.comsol.com stockholm, Sweden
[30] Bloch F 1946 *Phys. Rev.* **70** 460
[31] Parnell S R, Woolley E B, Boag S and Frost C D 2008 *Measurement Science and Technology* **19** 045601
[32] Guo S 2008 *Electrodynamics* 3rd Ed. (Beijing: Higher Education Press) (in Chinese)
[33] Qin Z, Huang C, Buck Z, Kreuzpaintner W, Amir S, Salman A, Ye F, Zhang J, Jiang C, Wang T, *et al.* 2021 *Chin. Phys. Lett.* **38** 052801
[34] Batz M, Bae?ler S, Heil W, Otten E, Rudersdorf D, Schmiedeskamp J, Sobolev Y and Wolf M 2005 *Journal of Research of the National Institute of Standards and Technology* **110** 293
[35] Tong X, Jiang C, Lauter V, Ambaye H, Brown D, Crow L, Gentile T, Goyette R, Lee W and Parizzi A 2012 *Rev. Sci. Instrum.* **83** 075101
[36] Jiang C, Tong X, Brown D, Glavic A, Ambaye H, Goyette R, Hoffmann M, Parizzi A, Robertson L and Lauter V 2017 *Rev. Sci. Instrum.* **88** 025111